Supporting Information

Engineering the CeO_2 Layer on Gold Nanopyramids for Enhanced Near-infrared Photothermal Conversion

Yifan Wang,[a,b,#] Hong Qu,[e,f,#] Guofeng Zhang,[a] Wusong Geng,[a] Lifeng Hang,[e,*] Tao Zhang,[c,d,*] and Yue Li[a,c,*]

[a] Mr. Y. Wang, Mr. G. Zhang, Mr. W. Geng, Prof. Y. Li
Key Laboratory of Materials Physics, Institute of Solid State Physics, HFIPS, Chinese Academy of Sciences, Hefei 230031, P.R. China.
E-mail: yueli@issp.ac.cn

[b] Mr. Y. Wang
University of Science and Technology of China, Hefei, 230026, P.R. China

[c] Prof. Y. Li
School of Physical Science and Technology, Tiangong University, No. 399 BinShuiXi Road, XiQing District, Tianjin 300387, P.R. China

[d] Dr. T. Zhang
School of Physical and Mathematical Sciences, Nanyang Technological University,
21 Nanyang Link, Singapore 637371, Singapore
E-mail: tao.zhang@ntu.edu.sg

[e] Dr. H. Qu, Prof. L. Hang
Department of Medical Imaging, Guangdong Second Provincial General Hospital, Jinan University, Guangzhou 518037, P.R. China
E-mail: hanglf@ustc.edu.cn

[f] Dr. H. Qu
Department of Nuclear Medicine, The First Affiliated Hospital (Southwest Hospital) of Army Medical University, Chongqing, 400038, P.R. China.

Experimental Section

Materials

Chloroauric acid ($HAuCl_4 \cdot 4H_2O$, 99.9%), silver nitrate ($AgNO_3$, ≥99.8%) ethylene glycol (EG, ≥99.5%), hydroquinone (HQ, ≥99.0%), trisodium citrate dihydrate ($C_5H_5NaO_7 \cdot 2H_2O$, ≥99.5%) and sodium hydroxide (NaOH, ≥96.0%) were purchased from Sinopharm Chemical Reagent. Poly dimethyl diallyl ammonium chloride (PDDA, Mw = 100 000 - 200 000, 20.0 wt% in water) and cerium nitrate hexahydrate (≥99.95%) were purchased from Aladdin Scientific. Deionized water (DI water) was obtained from an ultrapure water purification system (Millipore Sigma Direct-Q5). All materials were used as received.

Synthesis of Au bipyramids and ACH NPs

First, sequentially introducing $HAuCl_4$ (0.25 mM, 15 μL), PDDA (25 mM, 1.2 mL), and $AgNO_3$ (1.6 mM, 48 mL) into 60 mL of EG. Oxygen was purged through the mixture for 10 min, followed by heating at 220°C in an oil bath for 3 h. The synthesized solution was left to stand for 24 h, after which the supernatant was decanted to isolate Au decahedrons. Subsequently, HQ (2 mM, 480 μL) and $HAuCl_4$ (1 mM, 60 μL) were added to the solution, thoroughly mixed, and heated at 50°C in a forced-air drying oven for 5 h. The resulting suspension was centrifuged (9,000 rpm, 15 min) multiple times with DI water, yielding Au bipyramids from the collected precipitates.

For ACH NPs synthesis, 100 mL of an aqueous mixture containing Au bipyramids and cerium nitrate hexahydrate (3.5 mM) was loaded into a three-necked flask. The pH was adjusted to 10 using NaOH under continuous nitrogen flow with mechanical stirring. Upon heating to 70°C, add cerium nitrate hexahydrate (2.5 mM) into the mixture, followed by further heating to 90°C for 5 h. The mixture was purified via iterative centrifugation (DI water, 6,000 rpm, 5 min) post reaction, with the final ACH NPs settlings obtained from the pelleted phase.

Characterization

The morphological features of the samples were characterized using a field-emission scanning electron microscope (FE-SEM, SU 8020). Further structural analysis was conducted via transmission electron microscopy (TEM, FEI Tecnai G2 F20) to examine morphology, high-resolution lattice imaging (HRTEM), selected-area electron diffraction (SAED), and energy-dispersive X-ray spectroscopy (EDS). TEM specimens were prepared by depositing aqueous

nanoparticle suspensions onto carbon-coated copper grids. UV-vis absorption spectra were acquired using a Shimadzu UV-2600 spectrophotometer. X-ray diffraction (XRD) patterns of the products were obtained on an X'Pert Pro MPD diffractometer with Cu-Kα radiation (λ = 1.54 Å). The chemical states of constituent elements were analyzed by X-ray photoelectron spectroscopy (XPS, Thermo ESCALAB250Xi). Elemental mass distribution was quantified through inductively coupled plasma optical emission spectroscopy (ICP-OES, ICP-7400).

The Photothermal and Photodynamic Effects of ACH NPs.

To investigate the photothermal performance of ACH NPs, a 1064 nm laser (1 W cm^{-2}) was used to irradiate water and ACH NPs aqueous dispersions of different concentrations for 4 min. Three laser on/off cycles were used to evaluate the photothermal stability of ACH NPs. The temperature of the solutions was monitored by a thermal camera. The photothermal conversion efficiency (η) were calculated according to the following equation:

$$\eta = \frac{hS(T_{Max} - T_{Sur}) - Q_{Dis}}{I(1 - 10^{-A})}$$

where $\boldsymbol{h}$ denotes the heat transfer coefficient, $\boldsymbol{s}$ is the surface area of the container, $\boldsymbol{T_{Max}}$ represents the maximum temperature reached by the solution, $\boldsymbol{T_{Sur}}$ is the ambient temperature, $\boldsymbol{Q_{Dis}}$ refers to the heat dissipation, $\boldsymbol{I}$ ndicates the laser power, and $\boldsymbol{A}$ stands for the absorbance.

In Vitro Cell Uptake.

Cellular uptake of ACH NPs by HONE-1 cells was evaluated using inductively coupled plasma mass spectrometry (ICP-MS). Briefly, HONE-1 cells were seeded in 24-well plates. After overnight incubation to allow cell adhesion, the original medium was replaced with fresh medium containing ACH NPs (400 μg/mL) for continued culture (0, 1, 2, 4, 6, and 8 h). Cells were then washed three times with PBS buffer, trypsinized, and resuspended in PBS buffer. Following cell counting, the cell pellets were obtained by centrifugation and digested with 0.5 mL aqua regia solution. Gold uptake was subsequently quantified using ICP-MS.

The Vitro Cytotoxicity Measurement of the ACH NPs

To assess the therapeutic efficacy of ACH NPs, in vitro cytotoxicity was evaluated. In accordance with the manufacturer's protocol, the cytotoxicity of the nanoparticles was determined using the Cell Counting Kit-8 (CCK-8). Briefly, human nasopharyngeal carcinoma

HONE-1 cells were cultured overnight in 96-well plates to allow adhesion. The cells were then treated with ACH NPs at varying concentrations (400, 200, 100, 50, and 0 μg mL^{-1}) for 24 h. Prior to measuring absorbance at 450 nm using a microplate reader, each well was pre-incubated with 10% CCK-8 solution for 1–2 h. Cell viability (%) was calculated using the formula:

$$Cell\ Viability = (A_E - A_B)/(A_C - A_B) \times 100\%$$

where A_E, A_C, and A_B represent the absorbance of experimental samples, untreated control samples, and blank controls, respectively. All experiments were performed in duplicate with six replicates per group.

Cell Viability and Live/Dead Staining

HONE-1 cells were first cultured overnight under standard conditions, then treated with varying concentrations (0, 50, 100, 200, and 400 μg mL^{-1}) of ACH NPs for 6 hours followed by 4 min irradiation with a 1064 nm laser (1 W cm^{-2}). After an additional overnight incubation, the phototoxicity of ACH NPs under laser treatment was assessed using the CCK-8 assay.

For Live/Dead staining, cells were co-incubated with 400 μg mL^{-1} ACH NPs for 6 h, irradiated under identical laser parameters, and subsequently cultured overnight. The cells were then stained with calcein-AM/propidium iodide (PI) following the manufacturer's protocol, with fluorescence microscopy imaging performed to visualize viability outcomes.

CT and Photoacoustic Dual-Modal Imaging

To evaluate the CT imaging potential of ACH NPs in vitro, nanoparticles at graded concentrations (0, 50, 100, 200, and 400 μg mL^{-1}) were prepared in EP tubes. Scans were performed using a small-animal CT system (UniteImage) at 70 kV and 100 mA. CT Hounsfield unit (HU) values were quantified via the manufacturer-provided workstation. For in vivo studies, HONE-1 tumor-bearing mice with uniform tumor volumes were selected. CT scans were conducted pre- and post-intratumoral injection of ACH NPs to monitor HU value changes at tumor sites. All experiments were performed in triplicate.

For photoacoustic imaging (PAI), we first measured the photoacoustic signal intensities of ACH NPs at identical concentrations (0, 50, 100, 200, and 400 μg mL^{-1}) and established a concentration-signal correlation curve. Subsequently, HONE-1 tumor-bearing mice were

subjected to PAI before and after intratumoral ACH NPs injection to evaluate signal variations at tumor location.

In Vivo Tumor Therapy.

Consistent with the protocol for in vivo CT imaging, HONE-1 tumor-bearing mouse models were established, and treatment was initiated when tumor volumes reached approximately 100 mm^3 (designated as Day 0). Mice were randomly divided into four groups (n = 5 per group): (1) PBS group (intratumoral PBS injection), (2) ACH NPs group (intratumoral nanoparticle administration), (3) Laser group (1064 nm laser irradiation at 1 W/cm^2 for 4 minutes), and (4) ACH NPs + Laser group (combined treatment). Infrared thermal imaging was employed to monitor real-time temperature changes at tumor sites during laser irradiation for the Laser and ACH NPs + Laser groups. Post-treatment observations continued for 14 days, with body weight and tumor dimensions recorded every 48 hours. After two weeks, mice were euthanized, and excised tumors were weighed, photographed, and processed for histological evaluation using hematoxylin and eosin (H&E) staining and Ki67 immunohistochemistry to assess tissue morphology and proliferative activity.

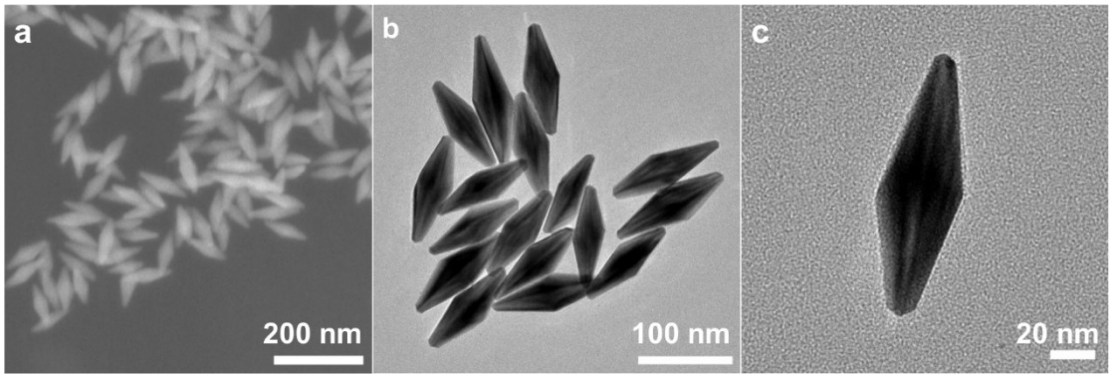

Figure S1. (a) SEM image, (b) TEM image and (c) lower magnification TEM image of Au bipyramids.

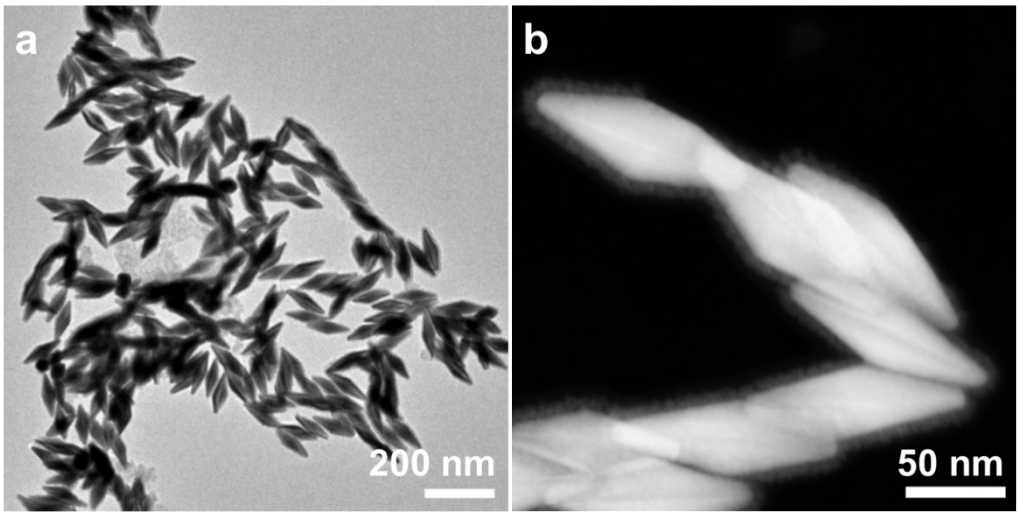

Figure S2. (a) low-magnification TEM image, and (b) HAADF-STEM image of ACH NPs.

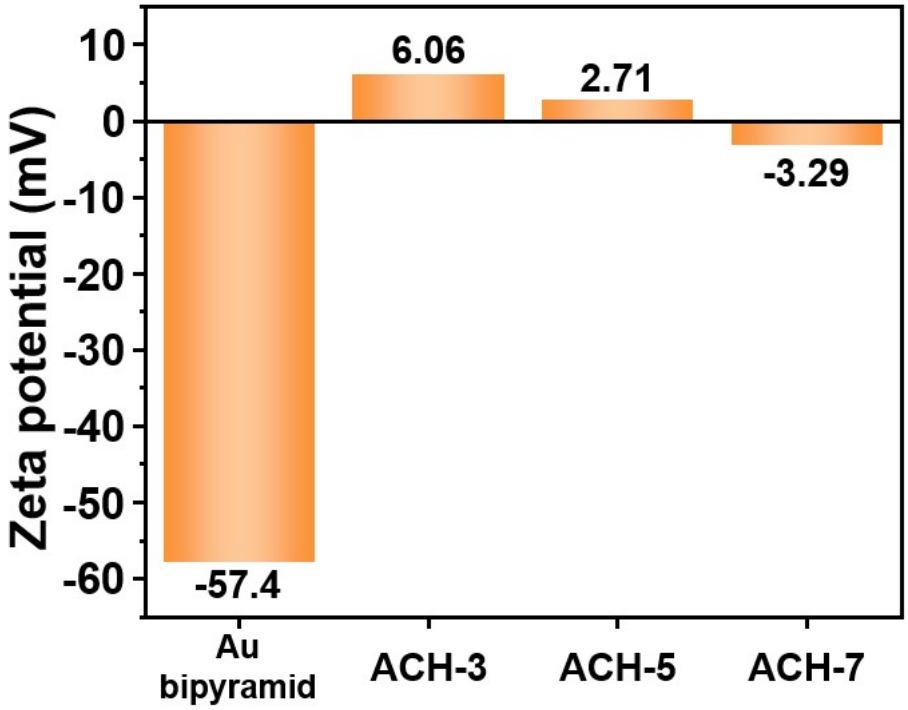

Figure S3. Zeta potential values of Au bipyramids, ACH-3, ACH-5 and ACH-7.

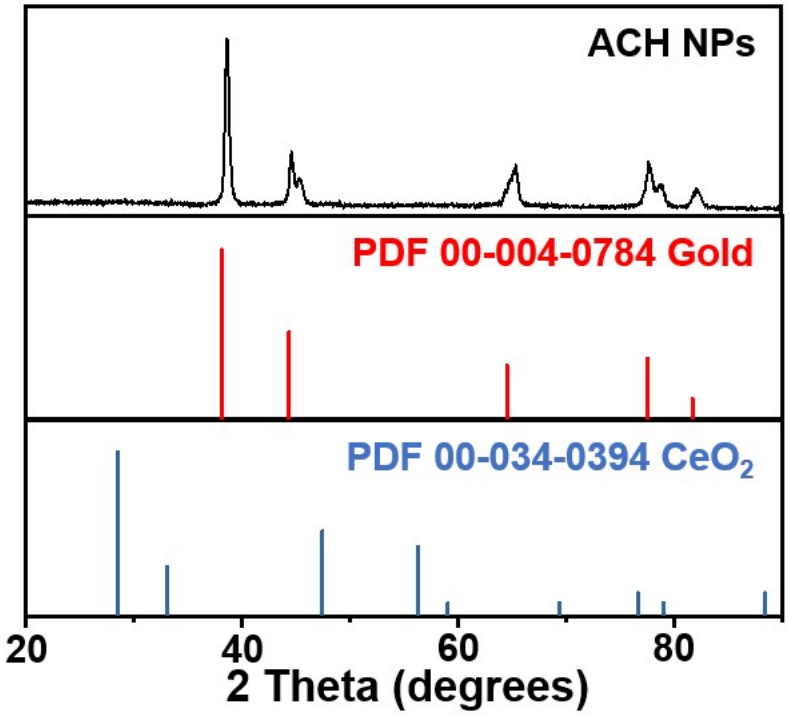

Figure S4. XRD pattern of ACH NPs overlaid with reference diffractograms for Au (PDF # 00-004-0784) and cubic fluorite-structured CeO_2 (PDF # 00-034-0394).

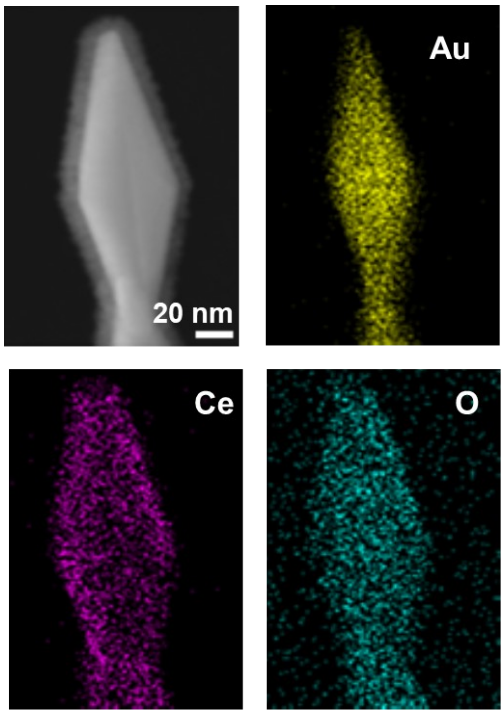

Figure S5. HAADF-STEM and the corresponding EDS mapping images of ACH.

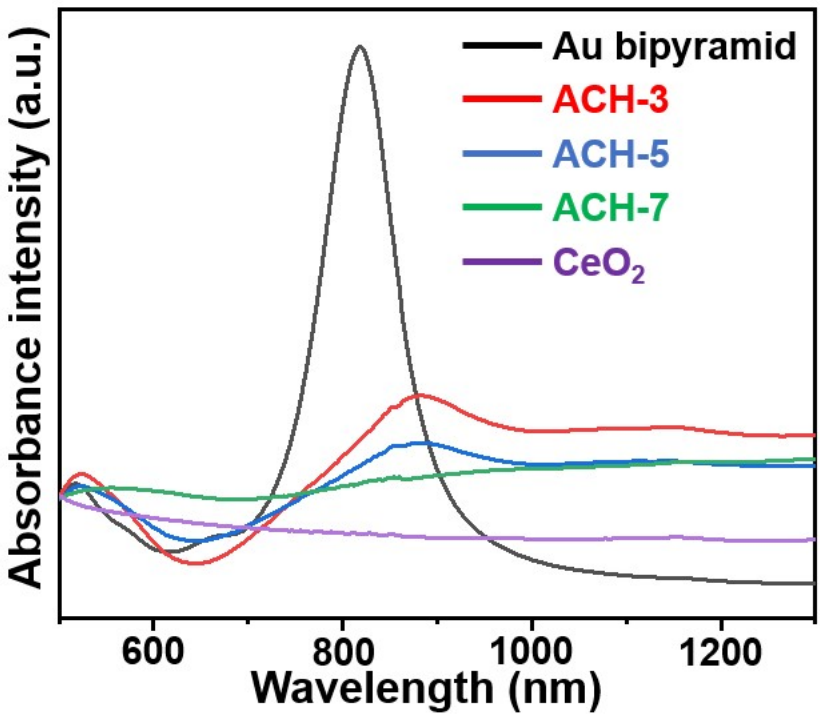

Figure S6. Comparative absorption spectra of Au decahedrons, ACH NPs synthesized with varying concentrations of cerium nitrate, and pure CeO_2 particles generated via an identical method.

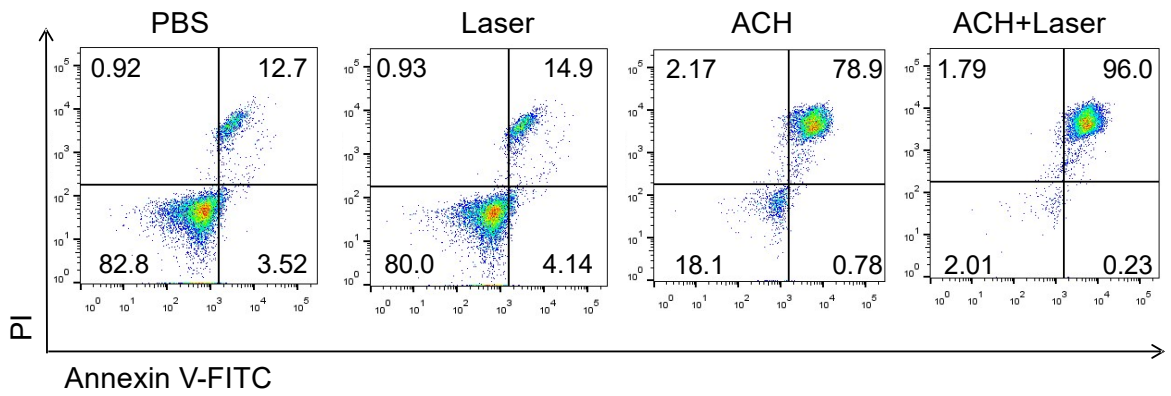

Figure S7. Flow cytometry apoptosis assay of HONE-1 cells stained with the membrane-associated protein V-FITC/PI after incubation with different formulations.

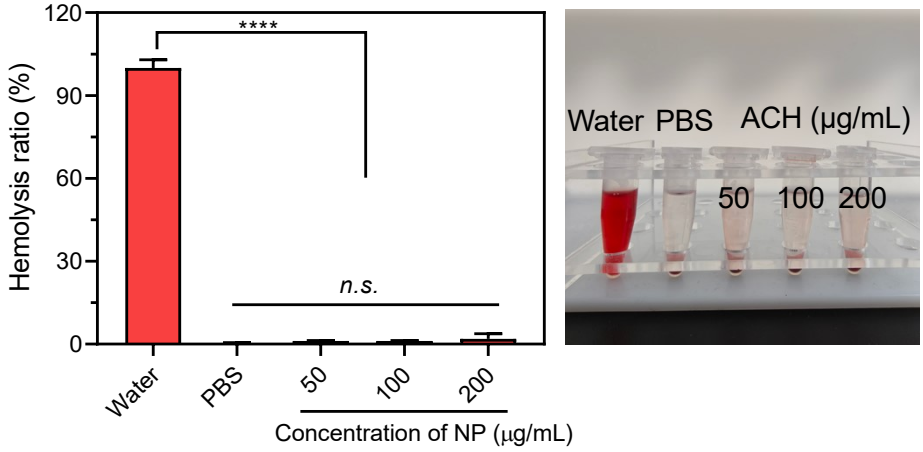

Figure S8. Hemolysis assay of the ACH with different concentration.

Table S1. Elemental contents of Au and Ce in ACH NPs synthesized with varying concentrations of cerium nitrate.

Type of ACH	Au content /wt.%	Ce content /wt.%	Molar ratio of Au to Ce
ACH-3	0.0693	0.0128	3.8
ACH-5	0.0739	0.0208	2.5
ACH-7	0.0208	0.0426	1